



Contents lists available at ScienceDirect

European Polymer Journal

journal homepage: www.elsevier.com/locate/europolj

Contributions of hard and soft blocks in the self-healing of metal-ligand-containing block copolymers

Ranjita K. Bose^a, Marcel Enke^{b,c}, Antonio M. Grande^a, Stefan Zechel^{b,c},
Felix H. Schacher^{b,c}, Martin D. Hager^{b,c}, Santiago J. Garcia^{a,*}, Ulrich S. Schubert^{b,c},
Sybrand van der Zwaag^a

^a Novel Aerospace Materials, Faculty of Aerospace Engineering, Delft University of Technology, Kluyverweg 1, Delft 2629HS, Netherlands

^b Laboratory for Organic and Macromolecular Chemistry (IOMC), Friedrich Schiller University Jena, Humboldtstr. 10, 07743 Jena, Germany

^c Jena Center for Soft Matter (JCSM), Friedrich Schiller University Jena, Philosophenweg 7, 07743 Jena, Germany

ARTICLE INFO

Keywords:

Self-healing polymer
Metallopolymer
Block-copolymer
Rheology
Supramolecular network

ABSTRACT

The main aim of this work is to study the respective contribution of the hard and soft blocks of a metal-ligand containing block copolymer to the self-healing behavior. To this aim, different block copolymers containing terpyridine were synthesized using reversible addition-fragmentation chain transfer (RAFT) polymerization. These block copolymers consisted of polystyrene as the hard block, *n*-butyl acrylate (BA) as soft block and terpyridine units as the ligand moiety placed at different locations in the soft block. These block copolymers were complexed with manganese(II) chloride to introduce transient crosslinks and, thus, self-healing behavior. Homopolymers with the hard and soft block only were also synthesized and tested. A quasi-irreversible crosslinking, *i.e.* by using nickel(II) nitrate, was performed in order to study the dynamics of the permanently (strongly) crosslinked network. Rheological master curves were generated enabling the determination of the terminal flow in these networks and the reversibility of the supramolecular interactions. Additionally, the macroscopic scratch healing behavior and the molecular mobility of the polymer chains in these supramolecular networks were investigated. A kinetic study of the scratch healing was performed to determine the similarities in temperature dependence for rheological relaxations and macroscopic scratch healing. In our previous work, we have explored the effect of strength of the reversible metal-ligand interaction and the effect of changing the ratio of hard to soft block. This work goes further in separating the individual contributions of the hard and soft blocks as well as the reversible interactions and to reveal their relative importance in the complex phenomenon of scratch healing.

1. Introduction

Block copolymers have been widely investigated due to the possibility of obtaining unique combinations of properties resulting from the different blocks not obtainable in random copolymers. For several decades, a number of research groups have reported on microphase separation of block copolymers [1–3]. The tunable synthesis of block copolymers can be used for wide-ranging applications such as stimuli responsive polymers [4–8], controlled drug delivery [9–11], and controlled permeability [12,13]. In recent years, block copolymer networks featuring self-healing ability have been investigated [14–16]. A key challenge in the design of

* Corresponding author.

E-mail address: s.j.garciaespallargas@tudelft.nl (S.J. Garcia).

<http://dx.doi.org/10.1016/j.eurpolymj.2017.06.020>

Received 10 April 2017; Received in revised form 12 June 2017; Accepted 15 June 2017

Available online 16 June 2017

0014-3057/ © 2017 The Authors. Published by Elsevier Ltd. This is an open access article under the CC BY license (<http://creativecommons.org/licenses/by/4.0/>).

intrinsic self-healing polymers is to enable temporary mobility of the polymer network using reversible bond formation while at the same time maintaining the structural integrity of the network. By the incorporation of two distinct polymer blocks with a different viscoelastic behavior, a balance between the two competing properties: mechanical robustness of the glassy block and viscous flow of the soft block can be achieved resulting in an enhancement of the overall material performance.

Intrinsically healable polymers have reversible chemical or physical linkages incorporated within the polymer structure and, consequently, do not require any additional healing agent such as a solvent, catalyst or monomer [17]. Examples of reversible chemical and physical linkages are Diels-Alder reactions [18–23], hydrogen bonding interactions [24–27], ionic clusters in ionomers [28–33], and metal-ligand bonds [26,34–39], which are also used in this contribution. Self-healing behavior is achieved *via* a thermally reversible bond between the metal cation and a terpyridine ligand [40]. These supramolecular interactions can have a range of strengths, directionality as well as a variety of coordination geometries and reversibility [37,41–44]. As reported previously, the dynamics of reversible crosslinks is the primary influencer of the bulk viscosities and, thus, of the resulting healing behavior in supramolecular networks [45].

In this work, we designed a supramolecular block copolymer, in which the soft block bears the reversible moieties. Polystyrene is used as the hard block and the soft block consists of *n*-butyl acrylate (BA) and the ligand moiety (terpyridine). Control experiments were performed by using nickel(II) nitrate resulting in a quasi-irreversible crosslinking as well as by synthesizing homopolymers of the hard or soft block. We used micro-scratch testing and image analysis of the disappearing scratches to quantify self-healing and its kinetics. We performed rheological experiments to study the relaxations of the transient interactions and the polymer backbone. Time-temperature superposition enables us to construct two master curves to analyze the network response over a broad range of time scales. The temperature dependence of the shift factors was used to demonstrate the mechanistic correspondence for rheology and scratch healing. Our previous publications have established the effect of using metal salts of varying complexation strengths [46] as well as the effect of changing the position and ratio of the hard and soft blocks [47]. However in this work we study in detail the individual contribution of the hard and soft blocks as well as the correlation of rheological behavior to macroscopic scratch healing.

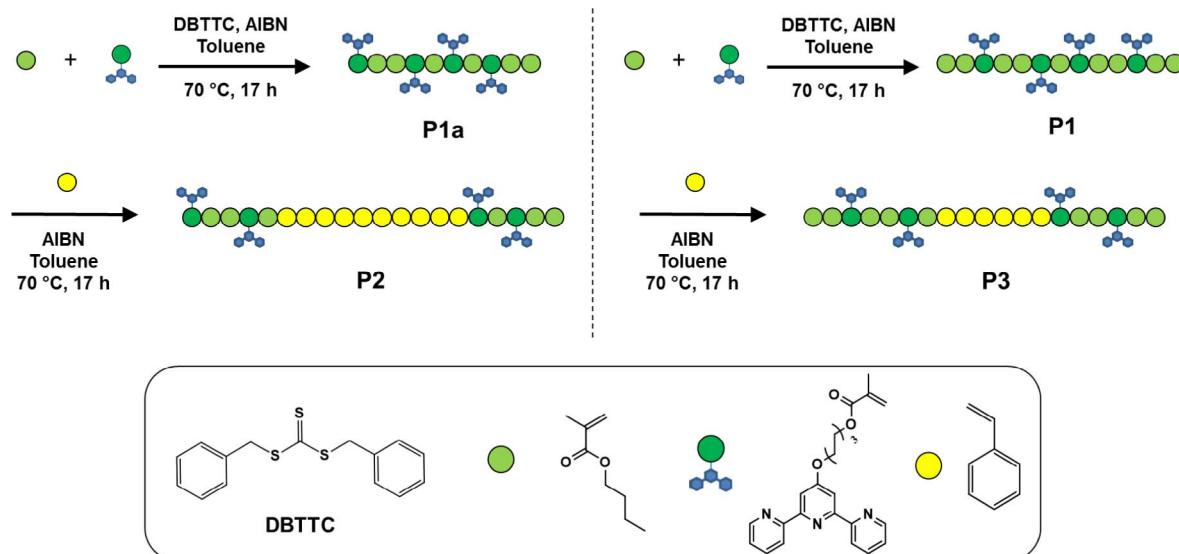
2. Experimental

2.1. Materials

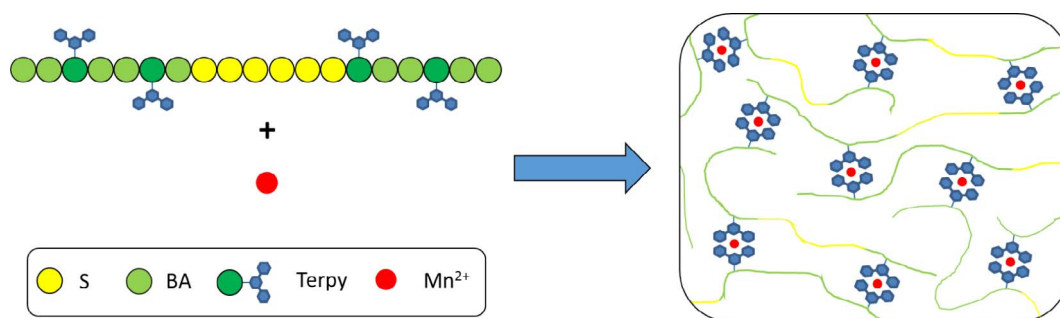
All chemicals used were purchased from Fluka, HetCat, Aldrich, and TCI and used without further purification. 6-(2,2':6',2''-Terpyridin-4'-yloxy)-hexyl methacrylate was synthesized according to literature procedures [48]. For ease of reading, the polymers are referred to as P1 to P4 and the metallopolymers MP1 to MP4. P1 to P4 and MP2 and MP3 were prepared according to the literature [47]. *N*-Butyl acrylate and styrene were passed over a short neutral aluminum oxide plug before use. The solvents were dried by refluxing over sodium/benzophenone (toluene) or dried with calcium chloride (chloroform and triethylamine).

2.2. Polymer synthesis

The block copolymers discussed in this study were synthesized by RAFT-polymerization using *S,S*-dibenzyl trithiocarbonate (DBTTC) as chain transfer agent [47]. In the first step, *n*-butyl acrylate and the terpyridine monomer were copolymerized resulting in copolymers P1 and P1a (Scheme 1). Subsequently, the copolymers were utilized for the preparation of the block copolymers. For this



Scheme 1. Schematic representation of block copolymer synthesis of P2 (hard-soft block ratio: 1:1) and P3 (hard-soft ratio: 1:2).



Scheme 2. Schematic representation of crosslinking of the block copolymers with manganese(II) chloride (anions are omitted).

purpose, styrene was polymerized *via* RAFT-polymerization using copolymers **P1/P1a** as macro-CTA, which results in an A-B-A structure (**P2** and **P3**, [Scheme 1](#)). The proton NMR spectra and the FT-IR spectra of the block copolymers **P2** and **P3** are depicted in [Figs. SI 1–4](#). Furthermore, the SEC results as well as the results of the thermal analysis are summarized in [Table SI 1](#).

However, the ratio between the hard and the soft block was varied resulting in two different block copolymers (**P2** and **P3**). Finally, pure polystyrene without any functional group was synthesized for comparison (**P4**) according to a previous procedure [47]. The molecular weights of the block copolymers (**P2** and **P3**) are approximately 20,000 g/mol ([Table SI 1](#)). The other polymers (**P1** and **P4**) have a lower molecular weight because they represent the separate block of the block copolymers ([Table SI 1](#)). The copolymers **P1** to **P3** were utilized for the preparation of metallopolymers by crosslinking them by the addition of either manganese(II) chloride or nickel(II) nitrate ([Scheme 2](#)).

2.3. Synthesis of the metallopolymers **MP1** and **MP4**

In a 5 mL vial the desired amount of polymer was dissolved in 1 mL chloroform. A solution of the metal salt in 1 mL methanol was added. The amounts of polymer and of the metal salts used are listed in [Table 1](#). After dissolution of the polymer the solvents were slowly evaporated. The resulting metallopolymers were washed with 1 mL methanol to remove any uncomplexed salt and were subsequently dried *in vacuo*. The results of the elemental analysis and the thermal properties are provided in [Table 2](#).

2.4. Polymer characterization

2.4.1. Fourier transform infrared spectroscopy (FT-IR) and elemental analyses (EA)

FT-IR spectra were acquired on a Shimadzu IRAffinity-1 instrument utilizing the Specac Quest ATR Diamond sample holder. EA were carried out on a Vario El III (Elementar) elemental analyzer.

2.4.2. Size exclusion chromatography (SEC)

SEC measurements were performed using a Shimadzu system and involving a SCL-10A VP (system controller), DGU-14A (degasser), LC-10AD VP (pump), SIL-10AD VP (auto sampler), RID-10A (RI detector), PSS GRAM guard/1000/30 Å (column), DMAc + 0.21% LiCl (eluent), 1 mL/min at 40 °C (flow rate and temperature), poly(methyl methacrylate) [molar mass range: 505–981,000 g/mol] and polystyrene (standard) [molar mass range: 374–1,040,000 g/mol].

2.4.3. Thermal analysis

The TGA analysis was carried out under helium using a STA Netzsch 449 F3 Jupiter and the thermal fluxes during heating were measured on a Netzsch DSC 204 F1 Phoenix under a nitrogen atmosphere with a heating rate of 10 or 20 K/min.

2.4.4. Rheology

To determine the rheological behavior, the metallopolymers samples with 8 mm diameter, corresponding to the rheometer plate diameter, were prepared as follows. The polymers (80 mg) and metal salts (in stoichiometric amount) were weighed in a vial, into which 0.5 mL each of chloroform and methanol were added to dissolve the polymer and the salt, respectively. This solution was then drop cast onto the bottom plate of the rheometer to allow *in situ* crosslinking. The solvent mixture was subsequently evaporated in a temperature-controlled chamber attached to the rheometer at 30 °C overnight. The low temperature and the slow rate of evaporation

Table 1
Overview of the reaction details of the crosslinking reactions for **MP1** and **MP4**.

Metallopolymer	Used polymer	Amount of polymer [mg]	Used metal salt	Amount of metal salt [mg]	Ratio terpyridine/metal salt
MP1	P1	50.9	MnCl ₂	2.6	2:1
MP4	P4	50.6	Ni(NO ₃) ₂	1.8	2:1

Table 2
Overview of the elemental analysis results and thermal properties of **MP1** and **MP4**.

Metallo-polymer	Carbon [%]	Hydrogen [%]	Nitrogen [%]	Chloride [%]	DSC: T_g [°C]	TGA: T_d [°C]
MP1	65.65	8.64	2.10	1.41	11	291
MP4	71.98	8.34	1.92	–	16	303

ensured a bubble-free sample. The samples were then held isothermally at 150 °C for 2 h to ensure a complete crosslinking and equilibration of the polymers. The upper plate of the rheometer was then lowered onto the sample till the sample completely filled the gap between the plates, which typically resulted in a sample thickness of 0.7–0.8 mm. Oscillatory shear amplitude sweep tests were performed to determine the linear viscoelastic region of each crosslinked polymer. A constant strain of 0.1%, which is within the linear viscoelastic region of the sample, was used for the subsequent experiments. Oscillatory shear frequency sweep experiments from 10 Hz to 0.1 Hz were performed from temperatures of 150 to –30 °C at intervals of 5 °C, with an isothermal hold for 2 min prior to each temperature step. Time-temperature superposition principle was applied to the frequency sweep data to generate horizontally shifted master curves. The reference temperature for the superposition was chosen as 100 °C in the first instance. In order to compare the relaxations of the polymers at a similar temperature away from glass transition, a second set of superposition was created with T_{ref} as $T_g + 50$ °C. The plateau modulus and relaxation behavior were observed from the rheological master curves.

2.4.5. Scratch healing

Scratch healing behavior was quantitatively studied using a dedicated micro-scratch testing device (CSM micro-scratch tester). Using a 100 μm diameter Rockwell diamond tip, first a pre-scan at 0.03 N load was performed to gauge the height profile of the coating in the planned direction of the scratch. Subsequently, scratches with a total length of 5 mm were produced using a progressive load from 0.03 to 30 N along the length of the scratch. A load of 0.5 N and a scratching speed of 2.5 mm/min resulted in a smooth scratch with a typical width of 200 μm which enabled a clear microscopic analysis of the scratched area during healing. For the tests reported here, a constant load of 0.5 N was selected. The initial depth of such scratches was approximately 50 μm which given a typical coating thickness of 200 μm means that substrate confinement effects do not play a role. Scratches were made at room temperature. The samples were then shifted to the *in-situ* microscope and heated at a rate of 50 °C/min to 100 °C. Micrographs were recorded for the entire duration of the healing process. Quantitative image analysis using ImageJ was used to compute the scratch surface area remaining at any time. A constant contrast threshold was chosen per series of images to ensure consistency in scratch area quantification. Scratch healing was defined as:

$$\% \text{Scratch healing} = \left(1 - \frac{A_t}{A_i}\right) \times 100 \quad (1)$$

where A_t is the surface area of the scratch at a given time and A_i is the initial scratch area. The kinetics of scratch healing was measured for **MP3** at different temperatures of 100, 90, 80, 70, 60, and 50 °C. A horizontal shift factor was calculated to superimpose the isothermal scratch healing curves.

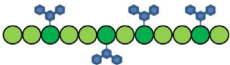




2.4.6. Small angle X-ray scattering (SAXS)

Small angle X-ray scattering (SAXS) measurements were performed on a Bruker AXS Nanostar (Bruker, Karlsruhe, Germany), equipped with a microfocus X-ray source (Incoatec μS_{Cu} E025, Incoatec, Geesthacht, Germany), operating at $\lambda = 1.54$ Å. A setup with three pinholes of 750 μm , 400 μm , and 1000 μm (with the 1000 μm hole closest to the sample) was used and the sample-to-detector distance was 107 cm. Samples were mounted on a metal rack using Scotch tape. The scattering patterns were corrected for the background (Scotch tape) prior to evaluation if necessary. Temperature ramps were performed from 20 to 120 °C in $\Delta K = 20$ steps. The measurement time per isothermal measurement was 2 to 4 h.

3. Results and discussion

The structure and the properties of the newly synthesized polymers used to fabricate the metallopolymers are listed [Table SI 1](#) and the values agree well with those reported earlier ([Table SI 3](#)) [47]. A detailed description of the block copolymers synthesis can be found in the experimental section. The resulting metallopolymers as well as their glass transition temperature (T_g) are displayed in [Table 3](#). **P1** represents the soft block consisting of *n*-butyl acrylate (BA) and 10% of the ligand moiety, with a molar mass of 14,800 g/mol (SEC) and a glass transition temperature (T_g) of –30 °C. In contrast, **P3** is a triblock copolymer ($M_n = 21,600$ g/mol), where polystyrene (PS) is introduced as the hard block as the middle domain. Consequently, the soft-block is separated into two parts (see also [Scheme 1](#)). **P3** has a T_g of –8 °C. Crosslinking with MnCl_2 of both polymers (**P1** \rightarrow **MP1**; **P3** \rightarrow **MP3**) results in an increase of the T_g . **MP1** has a T_g of 11 °C which is higher than that of **MP3** which has a T_g of –5 °C. On the one hand, the soft block is separated into two parts by the middle PS block resulting in a different crosslinking behavior compared with **P1**. In addition, the halving of the molar mass of the soft block results in a lower T_g of each soft block compared to **P1**, which also influences the T_g of **MP3**. It should be noted that we are comparing the T_g s of a soft crosslinked homopolymer (**MP1**) with a triblock copolymer (**MP3**), which shows phase-separation. The phase-separation can lead to nm-thick PS layers, which can also affect the T_g -value of **MP3** [49]. In addition, the metallopolymers are stable up to 320 °C ([Table SI 2](#), [Fig. SI 4–8](#)). TGA measurements also indicated that at 800 °C approximately

Table 3
Structure of the utilized metallopolymer **MP1** to **MP4** and their glass transition temperatures (T_g).

Metallo-polymer	Polymer used	Polymer structure	Hard vs. soft ratio	Metal salt	T_g [°C]
MP1	P1		–	MnCl ₂	11
MP2	P2		1:1	MnCl ₂	25
MP3	P3		1:2	MnCl ₂	–5
MP4	P3		1:2	Ni(NO ₃) ₂	16
–	P4		–	–	72

8–24% of the material is remaining. Thus, the exact metal content cannot be calculated from elemental analysis and TGA, respectively. The mechanical properties of the metallopolymer based on block copolymers were measured *via* nanoindentation and were published previously [47].

Within the last years, several studies investigating reversible interactions have focused on the dynamics in supramolecular polymers [50–55]. In order to understand the individual contributions of the hard and soft block, we investigated the molecular dynamics of these polymers. For this purpose, time–temperature superposition (TTS) is used as a tool in rheology to extend the experimental range of dynamical processes and to help understand phenomena at higher temperatures or longer timescales. If the oscillatory shear data at different temperatures can be shifted onto one master curve it is because the relaxations of all components of the network have the same scaling behavior with temperature. These materials are known as thermo-rheologically simple [56]. In complex polymer systems such as blends, block copolymers, or semi-crystalline polymers, a superposition is not always applicable due to the different temperature dependence of all the components of the polymer [57,58]. TTS was reported to fail at higher temperature for supramolecular networks, *i.e.* strongly associating hydrogen bonds [24,59]. The superposition fails most likely due to the differences in thermal dependence of the reversible interactions from the relaxation of the polymer backbone. In this work, TTS is found to be applicable to all the metallopolymer in the range of temperatures and frequencies explored. **P4**, which is a homopolymer of styrene, shows slight deviation from good superposition in the region of glass transition as well as terminal flow.

The first set of master curves, shown in Fig. 1, have been plotted with $T_{ref} = 100$ °C, based on the temperature used for the macroscopic healing tests. This allows us to compare the relaxations of all the networks at the same reference temperature. The crossover of G' and G'' is the transition of the network from a crosslinked, immobile state at higher frequencies to a reversible, mobile state at lower frequencies. The inverse of the crossover frequency is known as the supramolecular lifetime of the network or characteristic time of the terminal relaxation [28,59]. These values for each polymer are listed in Table 4. Both **MP2** and **MP3** show a broad relaxation, which can be deconvoluted to two relaxations arising from the glass transition and the reversible interactions. G' and G'' feature a crossover at low frequency before terminal flow is observed. **MP1** shows delayed onset of T_g in the extended frequency range, indicating the higher mobility of the *n*-butyl acrylate backbone polymer. The $G'-G''$ crossover at low frequency before terminal flow is also observed in **MP1**. **MP4** revealed a completely different behavior. In that case no $G'-G''$ crossover or terminal flow can be observed. This result confirms the completely crosslinked nature of the nickel(II) nitrate containing network, which is irreversible even at higher temperature (up to 200 °C) and on longer timescales. The strength of the metal salt and ligand bond is a crucial parameter in determining the dynamics of the reversible network. In the case of nickel(II) nitrate, the crosslinks are very strong, which halts the dynamics of the entire network, even not allowing the relaxation of the soft block.

The second set of master curves shown in Fig. 2 has been plotted with $T_{ref} = T_g + 50$ °C. Since each metallopolymer has a different T_g , the master curves have been plotted to a reference temperature that is equidistant to T_g in all cases to perform a better comparison between each system. The results of the comparison between the networks and the differences arising from the choice of reference temperature of superposition are shown in Table 4. The slopes of the terminal zone for **MP1**, **MP2**, **MP3** and **P4** are similar regardless of the reference temperature used to construct the master curves.

Interestingly, different evolution of the terminal relaxation for the different polymers can be extrapolated. While for **P4**, a classical Maxwellian relaxation is observed as highlighted by the slopes of G' and G'' in the low frequency region [60], for the other polymers, a substantial effect of both hard to soft block ratio and reversible bonds on the terminal relaxation is observed. Specifically, there is a net change in the elastic and viscous behaviors for **MP1** and **MP3** (different G' and G'' terminal slopes, see Table 4 with a relatively slower/delayed terminal relaxation process (Fig. 2). On the other end, the inclusion of soft blocks and reversible units in the polymer structure allowed a higher global mobility (lower T_g), which is a primary requirement for an efficient healing system.

In the case of **MP1**, **MP2** and **MP3**, which show complete self-healing, there is deviation from Maxwellian behavior. The slopes of G' and G'' are lower than 2 and 1, respectively. This behavior can be explained by the presence of supramolecular interactions in this range of time and temperature. Similar behavior has been reported for other supramolecular networks [52,55,61,62]. Other metallopolymer networks have shown a slope of 0.5 which indicates an intermediate state between the terminal response of viscoelastic materials and the plateau response of well-developed networks [63], resulting in weakly crosslinked dynamic networks. A closer look into the τ_b of **MP3** highlights the interplay of T_g and self-healing temperature. At $T_{ref} = 100$ °C, τ_b is 0.05 s and at $T_{ref} = 45$ °C, τ_b is

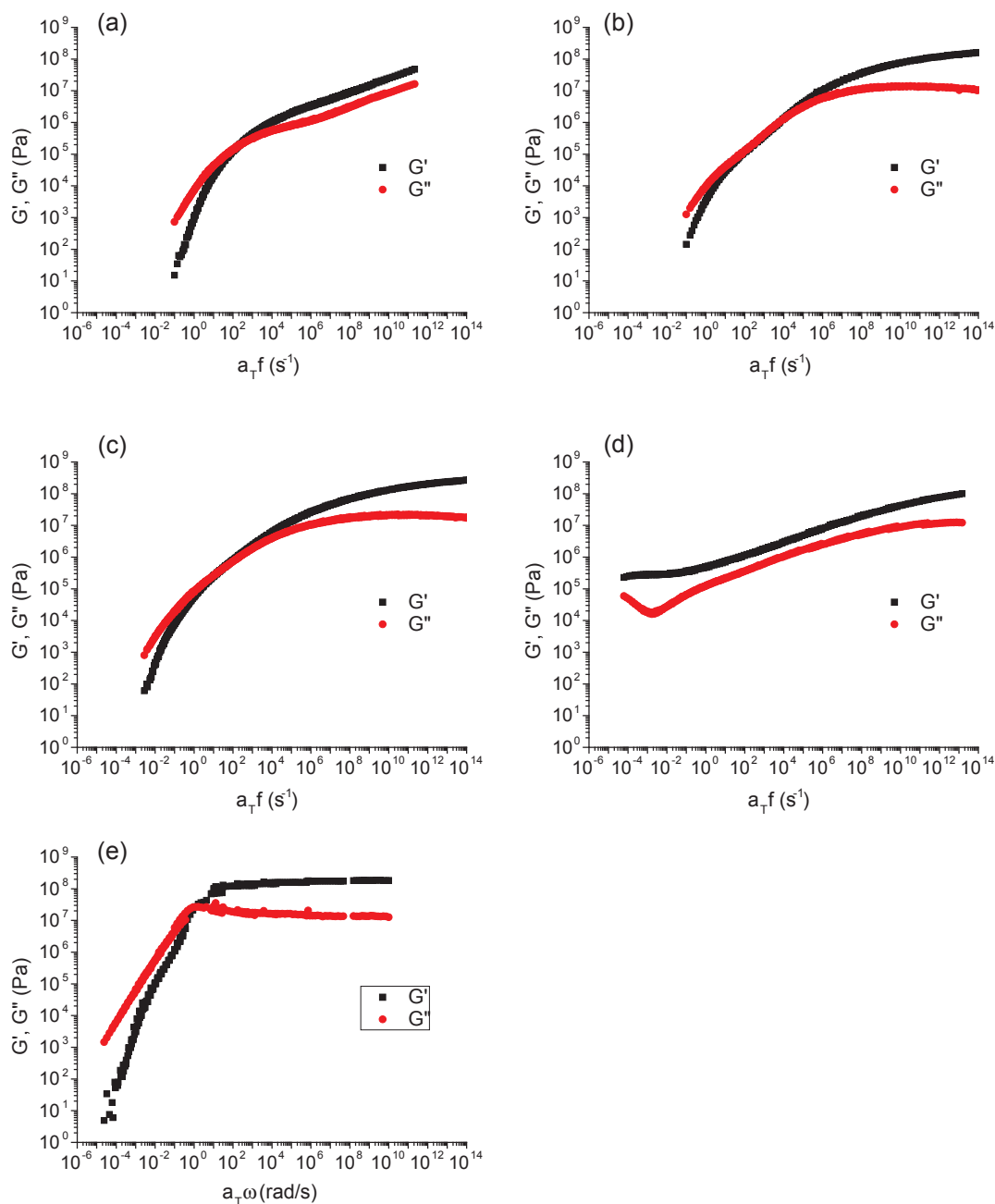


Fig. 1. Rheological master curves at $T_{ref} = 100\text{ }^{\circ}\text{C}$ showing the polymer relaxations in (a) **MP1**, (b) **MP2**, (c) **MP3**, (d) **MP4**, and (e) **P4** (see also Fig. SI 9).

4430 s. This shows the influence of healing temperature on the kinetics of self-healing. This is in good agreement with previous work where we have shown that ionomers with intermediate values of τ_b ($10 < \tau_b < 100$ s) demonstrate a favorable balance between mechanical robustness and self-healing ability [28]. In order to investigate the relaxations of the backbone polymer before complexing with metal salts, TTS was used. Fig. SI 10 shows the TTS curves of the backbone polymers **P2** (backbone block copolymer of **MP2**) and **P3** (backbone block copolymer of **MP3** and **MP4**).

The experiments were designed to study the macroscopic healing as well as the chain dynamics of the polymer network. In order to evaluate the macroscopic healing behavior, scratches were performed using a controlled load scratch tester, which ensured similar damage to all the samples. Optical micrographs and image analysis allowed us to define the healing efficiency as the area of the scratch relative to the initial area of the scratch. Scratches are made at room temperature at a constant load of 0.5 N, and each metallopolymer has a different mechanical stiffness at room temperature, which results in some variation in scratch dimensions as seen in the micrographs. As a consequence, the normalization of each scratch area to the initial area of the scratch ensures that we can still compare healing efficiencies of the different metallopolymers. The healing of all the samples was performed at 100 °C.

Table 4
Rheological parameters from TTS master curves for all the polymers (MP1 to MP4 and P4).

Polymer	$t_{\text{scratch healing}}$ [min]	$T_{\text{ref}} = 100\text{ }^{\circ}\text{C}$			$T_{\text{ref}} = T_g + 50\text{ }^{\circ}\text{C}$	
		τ_b [s]	Terminal slope of G'	Terminal slope of G''	τ_b [s]	T_{ref} [$^{\circ}\text{C}$]
MP1	20	0.005	1.60	0.91	1.12	60
MP2	45	0.03	1.03	0.68	0.99	75
MP3	5	0.05	1.40	0.85	4430	45
MP4	– ^a	– ^b	– ^b	– ^b	– ^b	65
P4	– ^a	0.18	1.96	0.98	2.8×10^{-4}	120

^a Does not heal.

^b No crossover is observed.

Micrographs recorded at different times are shown in Fig. 3. As published previously, MP2 showed complete scratch healing in 45 min, while in case of MP3 only 5 min were sufficient (optical micrographs of MP3 were published previously) [47]. This difference in the healing ability is attributed to the increased fraction of the soft block. MP1, which is a metallopolymer prepared from the pure soft block containing terpyridine moieties without any hard block, shows complete healing within 20 min. As a control experiment, MP4 featuring nickel(II)nitrate as crosslinker was used to show the impact of quasi-irreversible crosslinking of the network on the healing kinetics. This salt was chosen due to previously described non-healing behavior of a polymer network crosslinked with nickel-bis(terpyridine) [46]. MP4 indeed showed a negligible amount of recovery in 72 h (Fig. 3), which is found to be about 3% of recovery as shown in Fig. 4 upon scratch image analysis. This behavior suggests that nickel(II) nitrate acts as a quasi-irreversible crosslink, which does not enable healing in this polymer network according to previous described systems [46]. This finding is also in agreement with the rheology curves in Fig. 1(d), in which no terminal relaxation is observed for this metallopolymer.

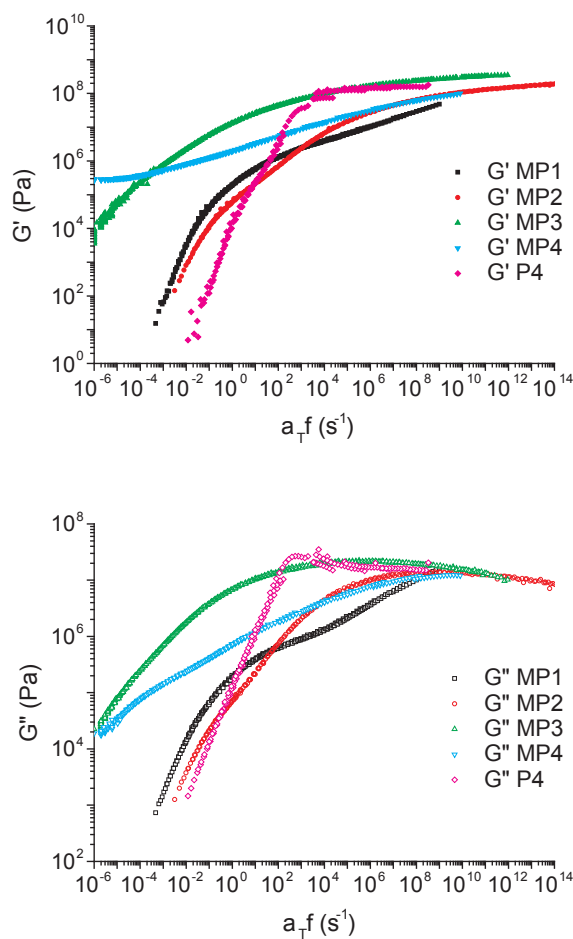


Fig. 2. G' and G'' of all polymers at $T_{\text{ref}} = T_g + 50\text{ }^{\circ}\text{C}$.

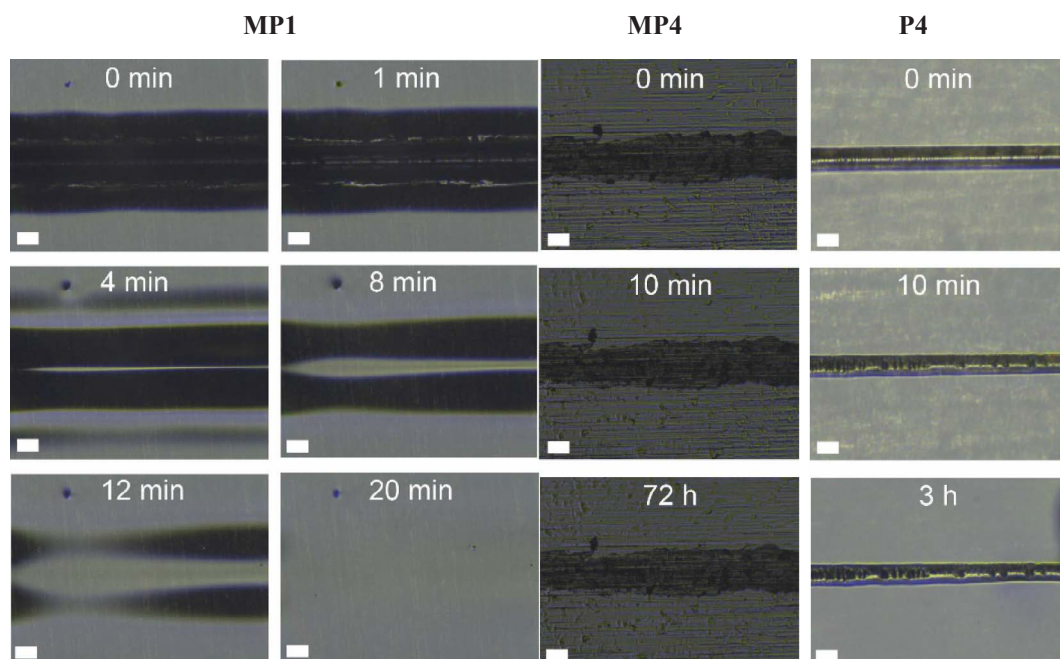


Fig. 3. Optical micrographs showing scratch healing in MP1, MP4 and P4 at 100 °C. Scale bars are 100 μ m.

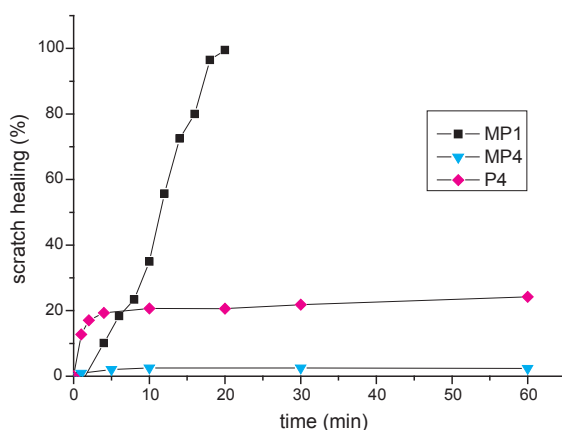


Fig. 4. Quantification of self-healing at 100 °C from image analysis of the scratch surface area.

P4, a homopolymer of polystyrene, reveals elastic recovery typical for polymers upon heating above their T_g [64]. The recovery of about 20% (as seen in Fig. 4) at an extended time of 3 h at 100 °C suggests that the polymer does not feature any self-healing ability at this temperature but only shows elastic recovery.

The bond lifetime from rheology and the timescale of scratch healing are not directly comparable. The former is a molecular time scale and the latter is a macroscopic phenomenon. Different types of damages will result in different time scales of healing. Therefore, the range of bond lifetimes from 10 to 100 s, which is seen as favorable range for healing in our previous work [28], cannot be directly translated to healing timescales. In order to overcome this limitation of direct comparison, we propose the following approach. In case of MP3, which showed the fastest healing, the kinetics of self-healing were also studied at different temperatures as shown in Fig. 5. The Arrhenius shift factors used to superpose the scratch healing data show a very close correspondence to the shift factors used to construct the rheological TTS master curves. Fig. 6 shows the two sets of data featuring a good overlap when plotted against the reciprocal temperature. A similarity between the fracture healing and rheological shift factors has also been reported recently for self-healing poly(urea-urethane) networks [65]. By fitting the shift factors with Arrhenius equation, two regions with different activation energy (E_a) can be distinguished: (i) above 50 °C with an associated activation energy of 47 kJ/mol ($E_{a,1}$) and (ii) below 50 °C with an activation energy $E_{a,2}$ of 86 kJ/mol. These results can be related to a change in the relaxation process due to the temperature dependent polymer arrangement as observed by SAXS experiments (see Fig. SI 4(b)). At low temperature chain movements are constrained while at high temperature (above 50 °C), the disappearance of domains at the nanoscale allows molecular motion, resulting in a lower activation energy for the flow of the polymer. Hence healing behavior and the polymer relaxations follow

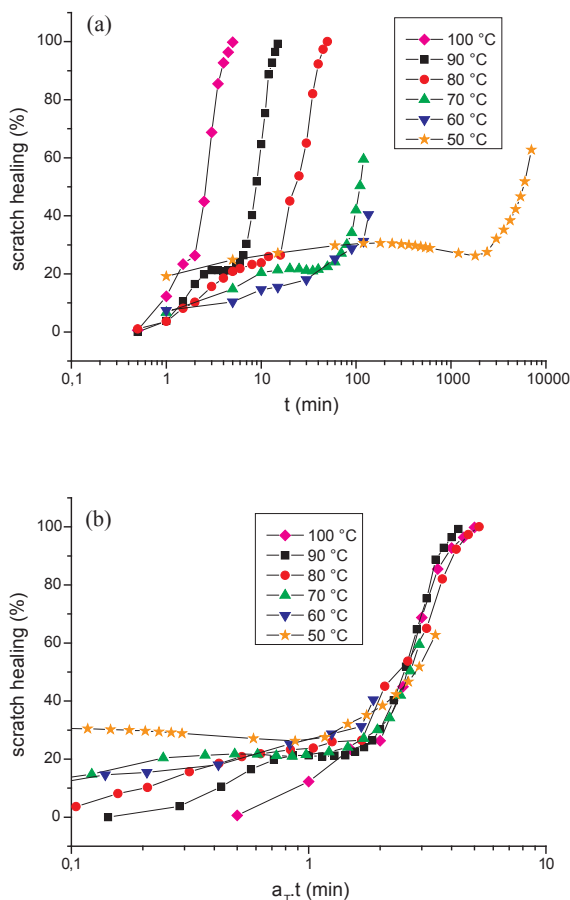


Fig. 5. (a) Kinetics of scratch healing of MP3 at different temperatures, and (b) superposed master curve of scratch healing kinetics. (Scratch healing at 100 °C, reproduced with permission from [47].)

the same temperature dependency and that the same molecular motions may govern both processes. Consequently, the viscoelastic and healing response are closely related, the latter can be considered as an intrinsic property of a polymer such as relaxation or creep and can be potentially studied with the same tools usually employed to investigate the viscoelastic behavior of a polymer (e.g., relaxation and retardation spectra, TTS).

All metallopolymers were further investigated with small angle X-ray scattering (SAXS) (Table SI 11). As expected, MP1 does not show any long range ordering. In case of MP4, no reflections are observed even at higher temperatures. This can be attributed to the addition of nickel(II) nitrate, which results in an irreversibly crosslinked network, wherein ordered phase separation is prevented.

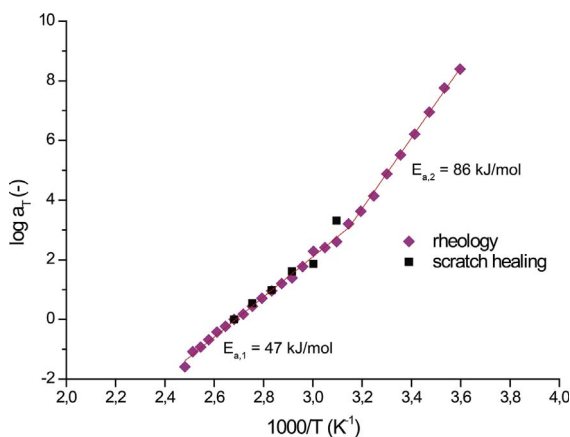


Fig. 6. Temperature dependence of shift factors used to construct rheological and scratch healing master curves for MP3.

However, both **MP2** and **MP3** show a broad reflection (Fig. SI 11), hinting towards phase separation occurring in bulk samples, even after crosslinking. Hereby, the domain spacing of 23 nm (**MP2**) and 26 nm (**MP3**) corresponds to the domain size within the bulk structure of these ABA triblock copolymers, different than values of 5–8 nm as reported in the literature for other metallopolymers, which presumably correspond to the formation of ionic clusters [34,46]. Within the temperature range accessible in our experiments (120 °C), no order–disorder transition was observable.

In summary, the block copolymer architecture, the glass transition temperature, the appearance or the kind of phase separation and the binding affinity of the metal–ligand complex have an individual influence on the self-healing behavior of the metallopolymers presented here. Therefore, all discussed influences should be taken into consideration in the design of self-healing polymers. The fact that the parameters feature a strong dependency on each other greatly complicates this analysis.

4. Conclusions

The main aim of this work was to study the contribution of the hard and soft segments of the block copolymer to the viscoelastic and self-healing behavior. The mobility during healing strongly depends on the block structure as seen from the rheology results. The slopes of the terminal relaxation show constrained dynamics with the introduction of various supramolecular interactions. **MP1**, **MP2** and **MP3** show different kinetics of healing in the macroscopic tests. These results are in agreement with the extent of terminal relaxation and supramolecular bond lifetime as determined by rheology. Changing the reference temperature of the TTS helps us to highlight the influence of healing temperature on the supramolecular network lifetime and, thus, on the kinetics of self-healing. **MP4** with quasi-irreversible metal–ligand interactions does not heal and also does not show terminal flow. This proves that the strength of the supramolecular interaction represents a key parameter that needs to be tuned to obtain healable polymers as required by different applications. **P4** with only PS block undergoes elastic recovery but does not heal fully. This indicates that supramolecular interactions are crucial for healing in these polymers. Thus for polymer networks to heal, the presence of reversible supramolecular interactions and the healing temperature suitably above T_g which provides sufficient network mobility are the limiting conditions. The shift factors used to construct the rheological and scratch healing master curves follow the same temperature dependence. The viscoelastic contributions of the hard and soft blocks as well as the reversible interaction show their relative importance in the complex phenomena of self-healing. These results can be extended to understand the healing in other supramolecular polymer networks. The rheological behavior of these supramolecular polymer networks should provide us an in-depth analysis of network mobility and self-healing.

Acknowledgment

The authors thank the Deutsche Forschungsgemeinschaft (DFG, SPP 1568) for funding within the framework of the priority program SPP 1568 “Design and Generic Principles of Self-healing Materials”. F. H. S. and U. S. S. acknowledge the Thuringian Ministry for Education, Science and Culture (TMBWK grant #B515-11028, SWAXS JCSM).

Appendix A. Supplementary data

Supplementary data associated with this article can be found, in the online version, at <http://dx.doi.org/10.1016/j.eurpolymj.2017.06.020>.

References

- [1] F.S. Bates, *Macromolecules* 17 (1984) 2607–2613.
- [2] R.D. Groot, T.J. Madden, D.J. Tildesley, *J. Chem. Phys.* 110 (1999) 9739–9749.
- [3] L. Leibler, *Macromolecules* 13 (1980) 1602–1617.
- [4] F. Chécot, S. Lecommandoux, Y. Gnanou, H.-A. Klok, *Angew. Chem. Int. Ed.* 41 (2002) 1339–1343.
- [5] F. Kohori, K. Sakai, T. Aoyagi, M. Yokoyama, Y. Sakurai, T. Okano, *J. Control. Release* 55 (1998) 87–98.
- [6] C.M. Schilli, M. Zhang, E. Rizzardo, S.H. Thang, Y.K. Chong, K. Edwards, G. Karlsson, A.H.E. Müller, *Macromolecules* 37 (2004) 7861–7866.
- [7] Y. Zhang, S. Chen, M. Pang, W. Zhang, *Polym. Chem.* 7 (2016) 6880–6884.
- [8] M.A.C. Stuart, W.T.S. Huck, J. Genzer, M. Muller, C. Ober, M. Stamm, G.B. Sukhorukov, I. Szleifer, V.V. Tsukruk, M. Urban, F. Winnik, S. Zauscher, I. Luzinov, S. Minko, *Nat. Mater.* 9 (2010) 101–113.
- [9] J.E. Chung, M. Yokoyama, M. Yamato, T. Aoyagi, Y. Sakurai, T. Okano, *J. Control. Release* 62 (1999) 115–127.
- [10] B. Jeong, Y.H. Bae, D.S. Lee, S.W. Kim, *Nature* 388 (1997) 860–862.
- [11] G. Kwon, M. Naito, M. Yokoyama, T. Okano, Y. Sakurai, K. Kataoka, *J. Control. Release* 48 (1997) 195–201.
- [12] K.T. Kim, J.J.L.M. Cornelissen, R.J.M. Nolte, J.C.M. van Hest, *Adv. Mater.* 21 (2009) 2787–2791.
- [13] C. Nardin, J. Widmer, M. Winterhalter, W. Meier, *Eur. Phys. J. E* 4 (2001) 403–410.
- [14] M.J. Barthel, T. Rudolph, A. Teichler, R.M. Paulus, J. Vitz, S. Hoepfner, M.D. Hager, F.H. Schacher, U.S. Schubert, *Adv. Func. Mater.* 23 (2013) 4921–4932.
- [15] J. Hentschel, A.M. Kushner, J. Ziller, Z. Guan, *Angew. Chem. Int. Ed.* 51 (2012) 10561–10565.
- [16] M.D. Chipara, M. Chipara, E. Shansky, J.M. Zaleski, *Polym. Adv. Technol.* 20 (2009) 427–431.
- [17] S.J. Garcia, *Eur. Polymer J.* 53 (2014) 118–125.
- [18] B.J. Adzima, H.A. Aguirre, C.J. Kloxin, T.F. Scott, C.N. Bowman, *Macromolecules* 41 (2008) 9112–9117.
- [19] R.K. Bose, J. Kötteritzsch, S.J. Garcia, M.D. Hager, U.S. Schubert, S. van der Zwaag, *J. Polym. Sci., Part A: Polym. Chem.* 52 (2014) 1669–1675.
- [20] G. Chen, M. Gupta, K. Chan, K.K. Gleason, *Macromol. Rapid Commun.* 28 (2007) 2205–2209.
- [21] J. Kötteritzsch, S. Stumpf, S. Hoepfner, J. Vitz, M.D. Hager, U.S. Schubert, *Macromol. Chem. Phys.* 214 (2013) 1636–1649.
- [22] Y.-L. Liu, C.-Y. Hsieh, Y.-W. Chen, *Polymer* 47 (2006) 2581–2586.
- [23] A.M. Peterson, R.E. Jensen, G.R. Palmese, *ACS Appl. Mater. Interfaces* 2 (2010) 1141–1149.

- [24] F. Herbst, D. Döhler, P. Michael, W.H. Binder, *Macromol. Rapid Commun.* 34 (2013) 203–220.
- [25] J.-M. Lehn, *Prog. Polym. Sci.* 30 (2005) 814–831.
- [26] T. Rossow, S. Hackelbusch, P. van Assenbergh, S. Seiffert, *Polym. Chem.* 4 (2013) 2515–2527.
- [27] F. Herbst, S. Seiffert, W.H. Binder, *Polym. Chem.* 3 (2012) 3084–3092.
- [28] R.K. Bose, N. Hohlbein, S.J. Garcia, A.M. Schmidt, S. van der Zwaag, *Phys. Chem. Chem. Phys.* 17 (2015) 1697–1704.
- [29] A.M. Grande, L. Castelnovo, L.D. Landro, C. Giacomuzzo, A. Francesconi, M.A. Rahman, *J. Appl. Polym. Sci.* 130 (2013) 1949–1958.
- [30] N. Hohlbein, A. Shaaban, A.R. Bras, W. Pyckhout-Hintzen, A.M. Schmidt, *Phys. Chem. Chem. Phys.* 17 (2015) 21005–21017.
- [31] S.J. Kalista, T.C. Ward, *J. Roy. Soc. Interface* 4 (2007) 405–411.
- [32] N.K. Tierney, R.A. Register, *Macromolecules* 35 (2002) 6284–6290.
- [33] R. Varley, in: S. Zwaag (Ed.), *Self Healing Materials*, Springer, Netherlands, vol. 100, 2008, pp. 95–114.
- [34] S. Bode, R.K. Bose, S. Matthes, M. Ehrhardt, A. Seifert, F.H. Schacher, R.M. Paulus, S. Stumpf, B. Sandmann, J. Vitz, A. Winter, S. Hoepfner, S.J. Garcia, S. Spange, S. van der Zwaag, M.D. Hager, U.S. Schubert, *Polym. Chem.* 4 (2013) 4966–4973.
- [35] N. Holten-Andersen, M.J. Harrington, H. Birkedal, B.P. Lee, P.B. Messersmith, K.Y.C. Lee, J.H. Waite, *Proc. Natl. Acad. Sci.* 108 (2011) 2651–2655.
- [36] J. Yuan, X. Fang, L. Zhang, G. Hong, Y. Lin, Q. Zheng, Y. Xu, Y. Ruan, W. Weng, H. Xia, G. Chen, *J. Mater. Chem.* 22 (2012) 11515–11522.
- [37] D. Mozhdzhi, S. Ayala, O.R. Cromwell, Z. Guan, *J. Am. Chem. Soc.* 136 (2014) 16128–16131.
- [38] M. Burnworth, L. Tang, J.R. Kumpfer, A.J. Duncan, F.L. Beyer, G.L. Fiore, S.J. Rowan, C. Weder, *Nature* 472 (2011) 334–337.
- [39] M. Enke, F. Jehle, S. Bode, J. Vitz, M.J. Harrington, M.D. Hager, U.S. Schubert, *Macromol. Chem. Phys.* (2017) 1600458-n/a.
- [40] S. Kupfer, L. Zedler, J. Guthmüller, S. Bode, M.D. Hager, U.S. Schubert, J. Popp, S. Grafe, B. Dietzek, *Phys. Chem. Chem. Phys.* 16 (2014) 12422–12432.
- [41] P. Wei, X. Yan, F. Huang, *Chem. Soc. Rev.* 44 (2015) 815–832.
- [42] D. Knapton, M. Burnworth, S.J. Rowan, C. Weder, *Angew. Chem. Int. Ed.* 45 (2006) 5825–5829.
- [43] F.S. Han, M. Higuchi, D.G. Kurth, *Adv. Mater.* 19 (2007) 3928–3931.
- [44] G.R. Whittell, M.D. Hager, U.S. Schubert, I. Manners, *Nat. Mater.* 10 (2011) 176–188.
- [45] W.C. Yount, D.M. Loveless, S.L. Craig, *Angew. Chem. Int. Ed.* 44 (2005) 2746–2748.
- [46] S. Bode, M. Enke, R.K. Bose, F.H. Schacher, S.J. Garcia, S. van der Zwaag, M.D. Hager, U.S. Schubert, *J. Mater. Chem. A* 3 (2015) 22145–22153.
- [47] M. Enke, R.K. Bose, S. Bode, J. Vitz, F.H. Schacher, S.J. Garcia, S. van der Zwaag, M.D. Hager, U.S. Schubert, *Macromolecules* 49 (2016) 8418–8429.
- [48] S. Bode, L. Zedler, F.H. Schacher, B. Dietzek, M. Schmitt, J. Popp, M.D. Hager, U.S. Schubert, *Adv. Mater.* 25 (2013) 1634–1638.
- [49] J.L. Keddie, R.A.L. Jones, R.A. Cory, *Europhys. Lett.* 27 (1994) 59–64.
- [50] R.K. Bose, N. Hohlbein, S.J. Garcia, A.M. Schmidt, S. van der Zwaag, *Polymer* 69 (2015) 228–232.
- [51] F. Liu, F. Li, G. Deng, Y. Chen, B. Zhang, J. Zhang, C.-Y. Liu, *Macromolecules* 45 (2012) 1636–1645.
- [52] N.E. Botterhuis, D.J.M. van Beek, G.M.L. van Gemert, A.W. Bosman, R.P. Sijbesma, *J. Polym. Sci., Part A: Polym. Chem.* 46 (2008) 3877–3885.
- [53] Y. Chen, H. Zou, M. Liang, P. Liu, *J. Appl. Polym. Sci.* 129 (2013) 945–953.
- [54] M. Hernández, A.M. Grande, W. Dierkes, J. Bijleveld, S. van der Zwaag, S.J. Garcia, *ACS Sustain. Chem. Eng.* 4 (2016) 5776–5784.
- [55] A. Susa, R.K. Bose, A.M. Grande, S. van der Zwaag, S.J. Garcia, *ACS Appl. Mater. Interfaces* 8 (2016) 34068–34079.
- [56] M.L. Williams, R.F. Landel, J.D. Ferry, *J. Am. Chem. Soc.* 77 (1955) 3701–3707.
- [57] R.H. Colby, *Polymer* 30 (1989) 1275–1278.
- [58] C. Dae Han, J.K. Kim, *Polymer* 34 (1993) 2533–2539.
- [59] S. Chen, D. Döhler, W.H. Binder, *Polymer* 107 (2016) 466–473.
- [60] W. Knoben, N.A.M. Besseling, L. Bouteiller, M.A. Cohen Stuart, *Phys. Chem. Chem. Phys.* 7 (2005) 2390–2398.
- [61] J.-L. Wietor, D.J.M. van Beek, G.W. Peters, E. Mendes, R.P. Sijbesma, *Macromolecules* 44 (2011) 1211–1219.
- [62] C.L. Elkins, T. Park, M.G. McKee, T.E. Long, *J. Polym. Sci., Part A: Polym. Chem.* 43 (2005) 4618–4631.
- [63] B. Yang, H. Zhang, H. Peng, Y. Xu, B. Wu, W. Weng, L. Li, *Polym. Chem.* 5 (2014) 1945–1953.
- [64] J.M. Vega, A.M. Grande, S. van der Zwaag, S.J. Garcia, *Eur. Polymer J.* 57 (2014) 121–126.
- [65] A.M. Grande, J.C. Bijleveld, S.J. Garcia, S. van der Zwaag, *Polymer* 96 (2016) 26–34.